ELSEVIER

Polymer 40 (1999) 5899–5905

polymer

Atomic force microscopy imaging of single polymer spherulites during crystallization: application to a semi-crystalline blend

Dimitri A. Ivanov*,[1], Bernard Nysten, Alain M. Jonas

Unité de Chimie et de Physique des Hauts Polyméres, Université Catholique de Louvain, place Croix du Sud, 1, B-1348 Louvain-la-Neuve, Belgium

Received 24 June 1998; received in revised form 3 November 1998; accepted 3 November 1998

Abstract

A new experimental setup designed to monitor by atomic force microscopy (AFM) the time evolution of a single micrometer-sized polymer spherulite during crystallization at elevated temperatures is presented. For the case of blends of poly(aryl-ether–ether–ketone), PEEK, with poly(ether–imide), PEI, it is shown how AFM can help visualizing the time sequence and space location of events occurring during polymer crystallization, specifically growth, branching and thickening of lamellar stacks (fibrils). This method complements other non-destructive techniques, e.g. optical microscopy, as it is able to examine the growth of very small crystals occurring for high degrees of supercooling. In addition, not only the overall spherulitic growth rate but also the growth rates of individual fibrils could be evaluated. The potential of the technique to evaluate crystallization near the surface by following the evolution of the surface roughness is briefly discussed.

Keywords: Semi-crystalline morphology; Polymer spherulite; Atomic force microscopy

1. Introduction

Static and dynamic studies of the structure and the crystallization of semi-crystalline polymers play an important role in the understanding of solid-state properties of polymers. Optical microscopy (OM) is one of the most common non-destructive techniques for such studies. OM helps not only to characterize spherulitic structure, but it can also provide information on the dynamics of polymer crystal growth [1–5]. However, the spatial resolution of OM and optical-range techniques [6] strongly restricts their application in the field of polymer morphology. Indeed, the size of basic structural elements in semi-crystalline polymers (crystalline lamellae and lamellar bundles) falls in most cases below the diffraction limits of these techniques [7]. Transmission electron microscopy (TEM) is in this respect better suited for detailed investigations on polymer microstructure [8]. However, it suffers from the requirement of chemical or physical modification of the sample (etching, staining, metal or carbon sputtering) and from frequent damages to the sample microstructure owing to electron irradiation. Therefore, TEM is essentially limited to static studies on polymers.

As a consequence, in order to dynamically follow polymer crystallization with a better resolution than OM, an alternative non-destructive technique was selected: atomic force microscopy (AFM). AFM recently proved its versatility in a large number of morphological studies on polymers [9–11]. In favorable instances, the AFM resolution is on par with that of electron microscopy. In these cases, AFM provides the possibility to examine semi-crystalline structures down to the level of lamellar and even molecular organization [12–14]. In addition, the advantages of AFM (high resolution and non-destructivity) offer a unique possibility for the repetitive examination of individual elements of the semi-crystalline structure. Such imaging performed on a single polymer spherulite during its isothermal crystallization and subsequent reheating to higher temperatures was first reported elsewhere [15,16]. The main technical difficulty of these measurements consists in the fact that typical ambient AFM setups preclude heating samples in situ to high temperatures (200°C or above), which was necessary for our application. Consequently, the imaging has to be performed under ambient conditions. To achieve repetitive imaging of the same spherulite and fibrils during crystallization at high temperature, a special setup was designed. This setup allowed to repeatedly restore the initial position and orientation of a sample (e.g., a thin polymer film) with respect to the scanner, after having performed thermal treatments on the samples ex situ. The

* Corresponding author.
E-mail address: divanov@ulb.ac.be (D.A. Ivanov)
[1] Present address: Unité de Physique des Polymères CP 223, Université Libre de Bruxelles, Boulevard du Triomphe, B-1050 Brussels, Belgium.

0032-3861/99/$ - see front matter
PII: S0032-3861(98)00812-X

reproducibility of sample positioning is in the range of a few tens of nm's, which is sufficient for our purposes.

The systems studied in this work are blends of PEEK with PEI that were extensively investigated in the past [17–21]. PEEK is a semi-crystalline semi-rigid polymer possessing several high performance properties, such as excellent thermal and chemical stability and outstanding mechanical properties, which are attractive for applications in fiber-reinforced composites [22,23] and automated device handling equipment [24]. PEI is also a high performance polymer [25,26], which is amorphous and fully miscible with PEEK in the amorphous state over all temperature and concentration ranges [17–19]. Upon crystallization, the growth of PEEK crystals mainly occurs in bundles, or lamellar stacks [27], consisting of several lamellae packed parallel to each other. Although the spherulite remains the major form of super-molecular organization in PEEK, this type of growth is, however, different from what is typically reported for flexible chain polymers, where growth, branching and splaying of isolated lamellae is often observed. In PEEK/PEI blends, PEI is rejected from the crystals of PEEK upon crystallization. Only a small amount of PEI is entrapped in the amorphous regions located between PEEK crystalline lamellae [18,28,29]. PEI is in fact rejected into interfibrillar or interspherulitic spaces. Consequently, PEI can be considered as an inert polymer diluent of PEEK. This diluent can be used to ''open up'' the semi-crystalline structure of PEEK, which is otherwise a puzzling object for morphological examinations owing to its extreme compactness. The addition of PEI to the PEEK/PEI blend increases the spatial separation of stacks of PEEK lamellae (i.e., lamellar bundles, or fibrils), rendering the microstructure more suitable for microscopic studies.

In the past, morphological studies on PEEK/PEI were performed with the help of transmission electron (TEM) [20,29,30] and polarized optical [19,20] microscopies. In the present work, our main purpose is to assess the new possibilities offered by the repetitive AFM imaging of the same PEEK spherulite during crystallization.

2. Experimental section

2.1. Materials

PEEK, grade Victrex 150P, was obtained from ICI. PEI, grade Ultem 1000, was received form General Electrics. The T_g's of the starting amorphous polymer (defined as the maxima of the imaginary part of the dynamic mechanical modulus at 1.0 Hz) were determined to be 143°C and 218.5°C for PEEK and PEI, respectively. Thin films of PEEK/PEI blend (55% (w/w) of PEEK) were used for the AFM measurements. This blend composition was selected for two reasons. On the one hand, the concentration of PEI in this blend is sufficiently high to ''open up'' the PEEK structure. On the other hand, the T_g of the amorphous blend remains low enough to provide a large temperature window for crystallization.

2.2. Preparation of PEEK/PEI thin films

PEEK was dried overnight at 80°C under vacuum. It was dissolved in benzophenone near its boiling point (305°C) during 10–15 min. at concentrations of about 0.1%. PEI was then added to PEEK by solution blending in benzophenone, and the mixtures were cast on freshly cleaved mica. The films were annealed during 10 min. at 400°C in order to evaporate the solvent and melt the polymer. Subsequent quenching to room temperature was performed by quickly sliding the mica substrates from the hot plate onto a metallic surface at room temperature. No traces of semi-crystalline structure could be detected in the quenched films by AFM. The continuous films possess flat surfaces with RMS roughness ranging between 4 and 8 Å and thicknesses (d) in the range 20–200 nm. The morphology of the thin PEEK/PEI films satisfies the two-dimensionality condition as $d/D_s \ll 1$, where D_s is the typical spherulites diameter. The isothermal crystallization of the blends was performed from the glassy state at different crystallization temperatures (T_c).

2.3. Atomic force microscopy

AFM topography images of the surfaces of thin PEEK/PEI films were obtained in contact mode (constant force) with 0.6 μm thick silicon nitride cantilevers ($k_c \sim 0.3\ \mathrm{Nm}^{-1}$), at ambient conditions with an Autoprobe CP (Park Scientific Instruments, Sunnyvale, CA). The appearance of a topographic contrast for the semi-crystalline films could be because of the density difference between amorphous and crystalline regions, and possibly also because of the special edge-on orientation of PEEK lamellae grown in thin films [31]. Based on the fact that thermal treatments cannot be carried out in situ, it was necessary to establish a special procedure in order to monitor the evolution of the same single spherulite during crystallization. For this purpose, copper grids for electron microscopy (Laborimpex) with $40 \times 40\ \mu\mathrm{m}^2$ labeled cells were used. The grids were glued on the backside of the mica substrate with a temperature-resistant epoxy-based thermoset resin (Ciba). These grids enabled the repetitive search of the same area of the samples by means of a reflection optical microscope. The further position refinement of the analyzed area was performed by AFM imaging using the coordinates of the centers of a few adjacent spherulites as references. Between two successive AFM observations, the samples were placed into an oven to perform the isothermal crystallization of the sample. Surface modifications of the sample surface were minimized by applying the smallest possible contact forces sufficient to produce a stable image (<10 nN). In addition, the amorphous regions of the blends are in the glassy state at ambient conditions, which decreases the probability to damage sample surface. The absence of artifacts owing to repetitive imaging was specifically checked for each sample

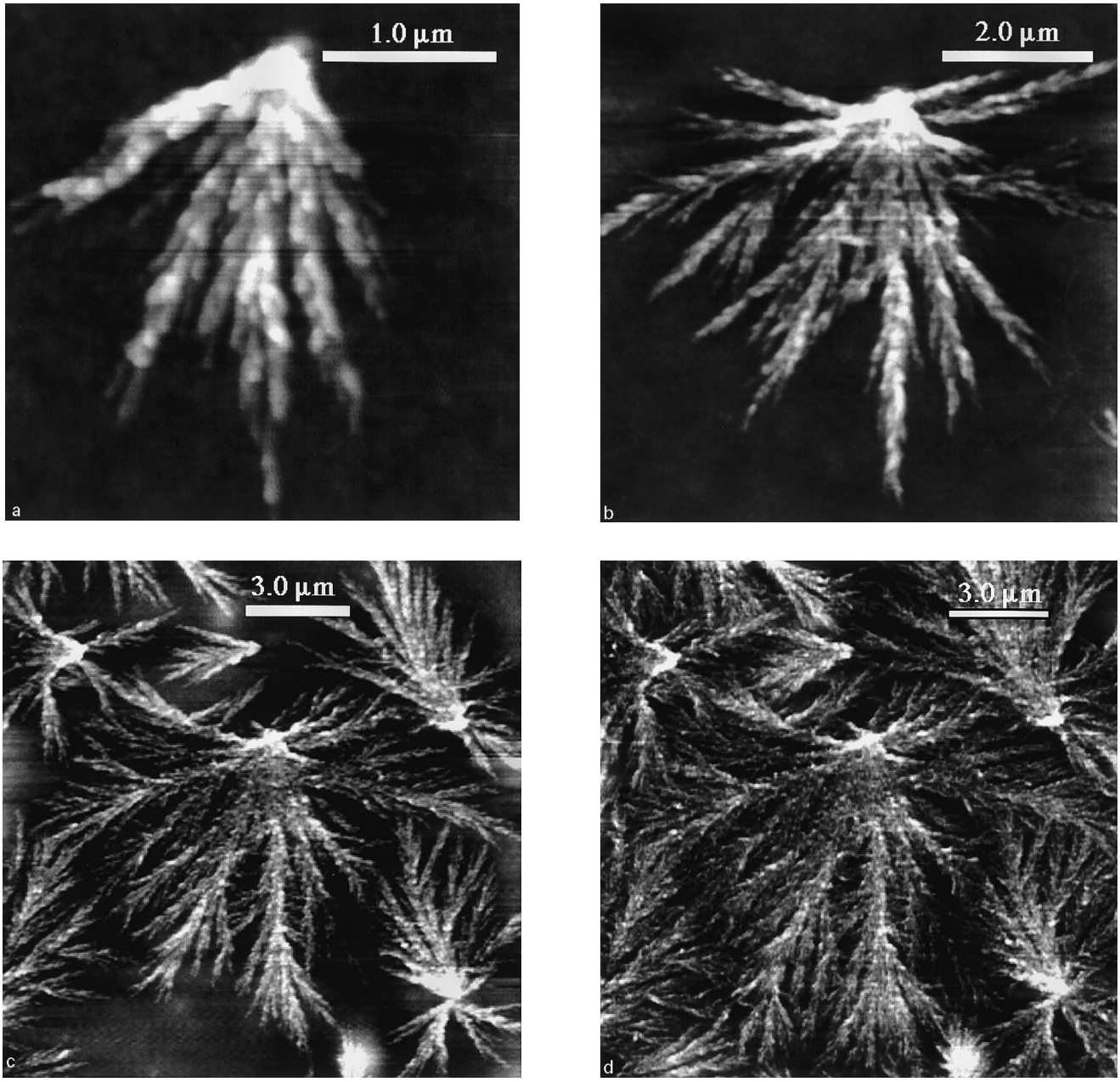

Fig. 1. AFM topographic images corresponding to the evolution of the same PEEK spherulite in a PEEK/PEI (55/45) thin film during crystallization at 190°C. Crystallization times: (a): 70 min.; (b): 140 min.; (c): 210 min.; (d): 280 min. The full grayscale corresponds to 110 Å (a,b) and 130 Å (c,d).

by comparing the appearance of the regions repetitively imaged with nearby regions that were not previously imaged by AFM.

2.4. Image analysis

The AFM image processing and analysis were performed using home-built procedures written in Wavemetrics Igor Pro (version 3.11). As topographic contrast resulting from the presence of spherulites often spanned only over about 100 Å, background effects (e.g. slight variation of film's thickness or intrinsic curvature of baselines owing to the bending motion of the scanner) could significantly perturb the image. This required writing specific correction procedures, based on an examination of the first and second derivatives of the image, to flatten the images. Height histograms and RMS roughness were then calculated on the flattened images.

To analyze the evolution of semi-crystalline morphology during crystallization, the image sequences corresponding to the growth of one isolated spherulite was treated as follows: The flattened images were first set to equal lateral scales using a bilinear interpolation procedure [32]. Preliminary superposition of images was then carried out by

hand. The refinement of the superposition of each image with respect to the others was automatically performed by maximizing the images product as a function of relative translation and rotation of one image with respect to the other. This numerical technique allowed to align successive images within ±20 nm and ±0.5° from each other.

3. Results and discussion

This section is organized as follows: In the first part, we report on one of the sequences of images of the same spherulite corresponding to the isothermal crystallization of a PEEK/PEI (55/45) blend. In the second and third parts, we discuss spherulitic evolution and, in particular, the possibilities offered by the repetitive imaging technique.

3.1. Repetitive AFM imaging of the same PEEK spherulite during crystallization

A typical sequence of AFM topography images corresponding to the evolution of a single PEEK spherulite is presented in Fig. 1(a)–(d). These images show the process of isothermal cold-crystallization of PEEK in a PEEK/PEI (55/45) thin film at a $T_c = 190°C$. The time interval between two successive measurements is equal to 70 min. The crystallization kinetics is very slow at this temperature. This fact can be explained by the close proximity of T_c to the glass transition temperature of the blend. Indeed, the T_g of amorphous PEEK/PEI blends is well described by the Fox equation [18]:

$$\frac{1}{T_g} = \frac{\omega_{PEEK}}{T_{g\ PEEK}} + \frac{1-\omega_{PEEK}}{T_{g\ PEI}}, \quad (1)$$

where ω_{PEEK} is the weight fraction of PEEK, and $T_{g\ PEEK}$ and $T_{g\ PEI}$ are the glass transition temperatures of both components. In the case of PEEK/PEI(55/45), it gives $T_g = 174°C$. It should be noted that repetitive quenching of the sample from this low crystallization temperature could not modify the structure of the sample or produce additional crystallinity, because of the strongly increasing diffusional constraints in the vicinity of T_g.

The very same spherulite easily recognized by its characteristic pattern of dominant fibrils spreading out from a central nucleus is imaged throughout the sequence. At the spherulitic scale, the classical progressive outward growth is observed. The growth is finally stopped by spherulitic impingement after 210–280 min. of crystallization (the somewhat smaller sizes of impinging peripheric spherulites (Fig. 1(c) and (d)) result from their later nucleation). At the sub-spherulitic scale, the radial growth and branching of individual PEEK fibrils is clearly visualized. Two characteristic features of this morphology can be pointed out:

(a) most of the PEEK fibrils are straight, only in some cases a slight curvature can be detected;

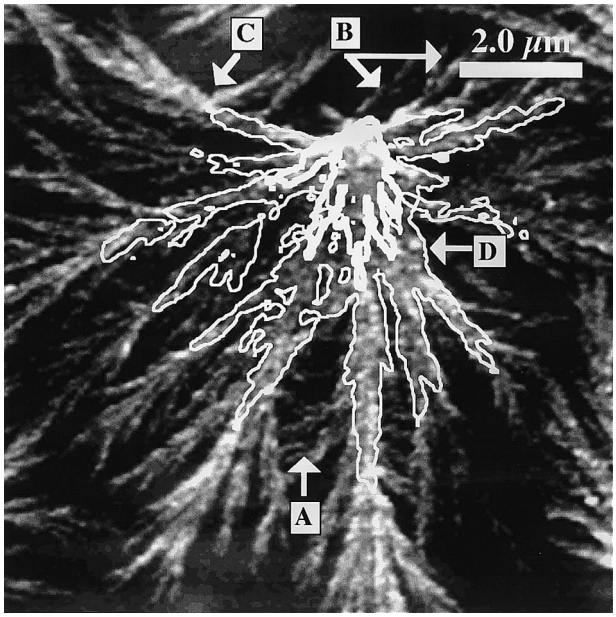

Fig. 2. Contours of a single spherulite after 70 and 140 min. crystallization at 190°C, superimposed on the image of the same spherulite after 210 min. crystallization (from Fig. 1(a)–(c)).

(b) the thickness of the fibrils is almost independent of the distance from the spherulites center.

This implies that fibril branching is an important mechanism required for the efficient filling of space by such structures.

At an early stage of crystallization, the immature PEEK spherulite shows a strong asymmetry (Fig. 1(a)) probably because of film thickness fluctuation near the seed. Upon crystallization, asymmetry progressively decreases as a result of branching. This evolution of spherulitic shape with time is similar but not identical to what is observed for pure polymers [8]. This is because of the fact that, in the blend, the crystalline growth mainly occurs through bundles separated by channels of amorphous PEI [27]. These bundles (or fibrils) consist of several lamellae which are packed parallel to one another [27].

The growth of several dominant fibrils was examined and was found to be linear up to the impingement, with a slight variation from one fibril to another. This means that the concentration of PEI at the growing tips is invariant with time. Hence, the rejected PEI does not escape ahead of the growing spherulitic front but accumulates inside the spherulites, between fibrils, as is typically observed for these blends [18,29].

One could expect effects as a result of the increase in the concentration of amorphous regions in PEI during crystallization to be locally most noticeable after the passage of the spherulitic growth front. In this case, the amorphous regions remaining between the fibrils are strongly enriched with PEI, resulting in a higher glass transition temperature which in some cases can even approach T_c leading to vitrification of these regions [33]. In the present case, this

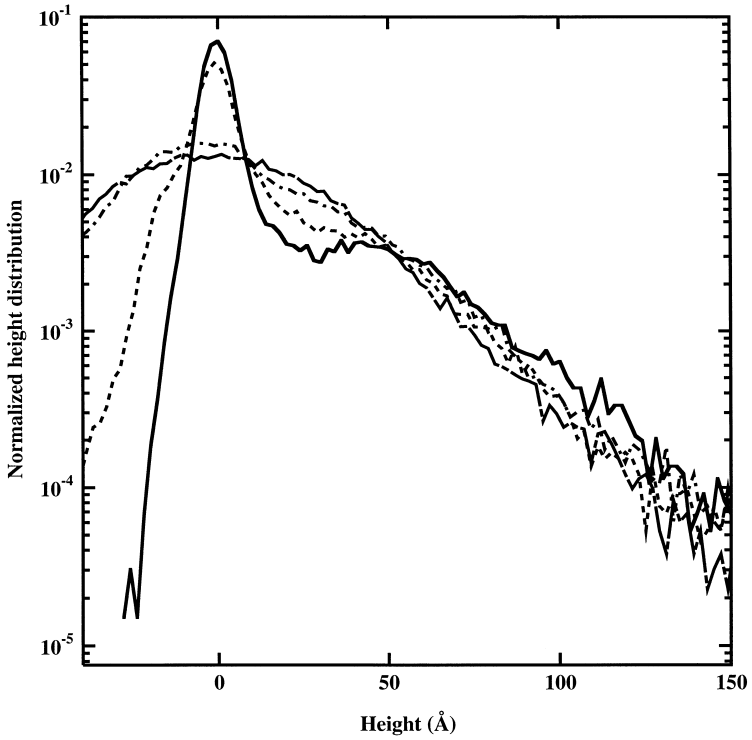

Fig. 3. Normalized height histograms corresponding to the images 1(a)–(d). Symbols: (a): solid line; (b): dashed line; (c): dashed-dotted line; (d): dashed-dotted line with longer dashes.

phenomenon however does not preclude further crystallization to occur in interfibrillar regions, as demonstrated in Fig. 2 where the images from Fig. 1 have been superimposed. The spherulite's contours corresponding to the crystallization times of 70 and 140 min. are shown in white to facilitate the comparison. In this figure, the growth of new fibrillar branches between already formed fibrils can be observed. This is particularly evident in the largest amorphous regions left after the passage of the spherulitic front, as in the regions marked A and D in Fig. 2, where new fibrils appear only after 210 min. of crystallization. The new fibrils either spread out from the central nucleus (B), or branch on already existing dominant fibrils (A,D). Backward fibrillar branching can also be observed on a slightly bowed fibril growing toward the upper left corner (C). The backward branching was described earlier for these systems by Lovinger et al. [20].

Apart from the formation of new fibrils in the PEI enriched regions, fibrillar thickening of previously formed fibrils also occurs, as can be seen by comparing the fibrils of the 70 min. spherulite to their more mature shape in the 140 min. spherulite (D), or in the 210 min. spherulite.

3.2. Roughness evolution during crystallization

The images shown in Fig. 1 can be analyzed in terms of integral parameters (e.g., RMS roughness). The corresponding height histograms plotted in semi-logarithmic coordinates (Fig. 3) reveal a bimodal shape up to 210 min. crystallization time. The relatively sharp distribution centered close to zero corresponds to amorphous regions, which are rather flat (RMS roughness ~4 Å). The progressive disappearance of this narrow distribution reflects the fading of the amorphous regions in benefit of growing spherulites. When the spherulites surface becomes dominant, the peak corresponding to the flat amorphous regions vanishes. Instead, a broader height distribution, corresponding to spherulites is observed. The larger width of this distribution mainly results from the density difference between crystalline and amorphous regions in spherulite leading to a partial depletion of material, as is typically observed in thin films [34]. The shoulder observed at larger heights after 70–210 min. crystallization times corresponds then to the fibril's surface, presenting a RMS roughness around 30 Å. The evolution of this shoulder could be used to follow the processes of crystal reorganization during subsequent heatings of the sample. However, for our isothermal crystallization, the shape of the crystal height histogram does not present any time variation, as expected as crystal reorganization should be negligible for such conditions [16]. It should be noted that this technique to evaluate crystallization by following the evolution of the surface roughness is not limited to thin films but can also be applied in studies focused on the transformations at the surface of bulk specimens.

Table 1
Radial growth rates of PEEK spherulites during isothermal crystallization of a PEEK/PEI (55/45) blend (thin film geometry)

T_c(°C)	G (nm s^{-1})
190	0.7
195	2.1
208	7.8

3.3. Temperature dependence of crystal growth rate

The repetitive imaging by AFM can also be applied to determine the temperature dependence of crystal growth rate. The development of the PEEK/PEI morphology was followed for three different T_c's. Corresponding values of the linear growth rates, G, were evaluated from these measurements (Table 1). G rapidly changes in this temperature region owing to the proximity of T_g. Generally, the growth of polymer crystals in this temperature range can be expressed as:

$$G = G_0 \exp\left(-\frac{U^*}{R(T_c - T_\infty)}\right), \quad (2)$$

where G_0 is an overall constant factor depending on the molecular weight, U^* is a transport activation energy, and T_∞ is a hypothetical temperature where all movements associated with viscous flow cease. In Eq. (2) we neglect thermodynamic terms that may be considered as constant in the restricted temperature window of the present cold-crystallization experiments [35]. The fitting of the experimental data (Table 1) with Eq. (2) using $T_\infty = T_g - 51.6$°C, gives $U^* = 1.55$ kcal/mol. The calculated U^* appears reasonable for PEEK, given the uncertainties about its exact value [36]. Hence, the determination of thermodynamic or kinetic parameters related to polymer crystal growth appears to be achievable by the AFM technique. However, the heavier implementation of our procedure as compared to OM restricts its use to extreme cases (mainly very small spherulites as obtained typically for crystallizations performed at large degrees of supercooling).

4. Conclusions

We have presented a new application of AFM that, provided a special sample preparation is carried out, allows to follow the time dependence of polymer crystallization at elevated temperatures. It was shown on a specific example how AFM could help in visualizing the patterns of events occurring during polymer crystallization, specifically growth, branching and thickening of lamellar stacks (fibrils) leading to the filling of space by the growing spherulites. As with OM, the integral radial growth rate of the spherulite can be determined, with the advantage that also the growth rate of different fibrils can be measured. Another interest of AFM is that its ability to determine the roughness of the samples allows us to follow the crystallization quantitatively. This could pave the way for specific studies on crystallization kinetics of polymers in the vicinity of free interfaces. However, the AFM technique has the inconvenience that its implementation in this mode is not as easy as that of OM. This, in practice, limits the application of this technique to very small spherulites found for high degrees of supercooling and not observable by OM.

Acknowledgements

We thank Prof. R. Legras for his support in our work. We are indebted to Mr. A. Gijbels (Ciba-Geigy N.V.) for the free delivery of a highly thermostable epoxide glue, to Dr. P.T. McGrail (I.C.I.) for providing us with PEEK and to Dr. C. Bailly (G.E. Plastics, Bergen op Zoom) for providing PEI. B.N. is a Research Associate of the Belgian National Fund for Scientific Research (F.N.R.S.).

References

[1] Huang T, Rey A, Kamal MR. Polymer 1994;35:5434.
[2] Tanaka H, Nishi T. Phys Rev A 1989;39:783.
[3] Martins JA, Cruz-Pinto JJC, Oliveira MJ. J Therm Anal 1993;40:629.
[4] Billingham NC, Calvert PD, Uzuner A. Polymer 1990;31:258.
[5] Hemsley DA. Applied polymer light microscopy. London: Elsevier, 1989.
[6] Born M, Wolf E. Principles of optics. Oxford: Pergamon Press, 1984.
[7] Wunderlich B. Macromolecular physics, 1. New York: Academic Press, 1973.
[8] Bassett DC. CRC Crit Rev Solid State Mater Sci 1984;12:97.
[9] Magonov SN, Cantow H-J. J Appl Polym Sci: Appl Polym Symp 1992;51:4.
[10] Legett GJ, Davies MC, Jackson DE, Roberts CJ, Tendler SJB. Trends in Polym Sci 1993;1:115.
[11] Harron HR, Pritchard RG, Cope BC, Goddard DT. J Polym Sci: Part B: Polym Phys 1996;34:173.
[12] Snétivy D, Vancso GJ. Polymer 1992;33:432.
[13] Goldbeck-Wood G, Fischer H, Barham PJ. Polym Bull 1995;35:183.
[14] Stocker W, Schumacher M, Graff S, Lang J, Wittmann JC, Lovinger AJ, Lotz B. Macromolecules 1994;27:6948.
[15] Ivanov DA, Jonas AM, Legras R. Bull Am Phys Soc 1996;41:395.
[16] Ivanov DA, Jonas AM. Macromolecules 1998;31:4546.
[17] Harris JE, Robeson LM. J Appl Polym Sci 1988;35:1877.
[18] Crevecoeur G, Groeninckx G. Macromolecules 1991;24:1190.
[19] Chen H-L, Porter RS. Polym Eng Sci 1992;32:1870.
[20] Hudson SD, Davis DD, Lovinger AJ. Macromolecules 1992;25:1759.
[21] Jonas AM, Russell TP, Yoon DY. Macromolecules 1995;28:8491.
[22] Nguyen HX, Ishida H. Polym Compos 1987;8:57.
[23] Searle OB, Pfeiffer RH. Polym Eng Sci 1985;25:474.
[24] Campbell RW, Tan W. Solid State Technology 1997;40:69.
[25] Johnson RO, Burlhis HS. J Polym Sci: Polym Symp 1983;70:129.
[26] White SA, Weissman SR, Kambour RP. J Appl Polym Sci 1982;28:2675.
[27] Lovinger AJ, Hudson SD, Davis DD. Macromolecules 1992;25:1752.
[28] Lee CH, Okasa T, Saito H, Inoue T. Polymer 1997;38:31.
[29] Jonas AM, Ivanov DA, Yoon DY. Macromolecules 1998;31:5352.
[30] Ivanov DA, Lipnik PDM, Jonas AM. J Polym Sci: Polym Phys 1997;35:2565.
[31] Lovinger AJ, Davis DD. J Appl Phys 1985;58:2843.

[32] Press WH, Teukolsky SA, Vetterling WT, Flannery BP. Numerical recipes in C. 2. Cambridge: Cambridge University Press, 1988.
[33] Ivanov DA, Jonas AM. J Polym Sci: Polym Phys 1998;36:919.
[34] Pearce R, Vancso GJ. Macromolecules 1997;30:5843.
[35] Day M, Deslandes Y, Roovers J, Suprunchuk T. Polymer 1991;32:1258.
[36] Medellin-Rodriguez FJ, Phillips PJ, Lin JS. Macromolecules 1995;28:7744.